

Document downloaded from:

<http://hdl.handle.net/10251/120662>

This paper must be cited as:

Smacchia, D.; Soto Pacheco, P.; Boria Esbert, VE.; Guglielmi, M.; Carceller Candau, C.; Ruiz-Garnica, J.; Galdeano, J.... (2018). Advanced Compact Setups for Passive Intermodulation Measurements of Satellite Hardware. *IEEE Transactions on Microwave Theory and Techniques*. 66(2):700-710. <https://doi.org/10.1109/TMTT.2017.2783383>



The final publication is available at

<http://doi.org/10.1109/TMTT.2017.2783383>

Copyright Institute of Electrical and Electronics Engineers

Additional Information

(c) 2018 IEEE. Personal use of this material is permitted. Permission from IEEE must be obtained for all other users, including reprinting/ republishing this

# Advanced Compact Setups for Passive Intermodulation Measurements of Satellite Hardware

Davide Smacchia, Pablo Soto, *Member, IEEE*, Vicente Boria, *Fellow, IEEE*, Marco Guglielmi, *Fellow, IEEE*, Carlos Carceller, *Member, IEEE*, Jesús Ruiz, Jaione Galdeano, and David Raboso

**Abstract**—This paper provides the guidelines for the practical development of novel advanced test beds for passive intermodulation (PIM) measurements. The proposed test beds are high-performance and flexible, allowing for the measurement of several PIM signals of different orders, with two or more input carriers. In contrast to classic test beds for satellite hardware, based on the cascaded connection of several elements, an integrated solution involving the minimum number of hardware pieces is proposed. The result is a lower number of flanged interconnections thus reducing residual PIM level and insertion losses. In addition, return loss degradation and harmful spurious generation in the interconnections are also avoided. Measurement test beds for conducted and radiated PIM, in both transmitted and reflected directions, are discussed, highlighting the benefits and drawbacks of each configuration. Design guidelines for the key components are fully discussed. Illustrative application examples are also reported. Finally, excellent experimental results obtained from low-PIM measurement setups, working from C band to Ka band, are shown, thus fully confirming the validity of the proposed configurations.

**Index Terms**—Intermodulation distortion, microwave filters, high-power filters, multiplexing, computer-aided engineering.

## I. INTRODUCTION

IN the last decades, the avoidance of passive intermodulation effects (PIM) has become a top-priority issue for communication satellites systems engineers, as a consequence of the ever more demanding payload requirements [1], [2]. PIM may, in fact, become an important source of performance degradation due to increased transmitted power levels for higher capacity links, together with the need for simultaneous operation in transmission (downlink) and in reception (uplink) at different frequency bands [3], [4]. In the scenario of

Manuscript received July 31, 2017; revised October 4, 2017; accepted November 29, 2017. This work has been funded by European Space Agency (ESA) through several R&D contracts, Ministerio de Economía y Competitividad (MINECO, Spanish Government) under research project TEC2016-75934-C4-1-R, and by the European High Power RF Space Laboratory.

This paper is an extended version from the IEEE MTT-S International Conference of Numerical Electromagnetic Modeling and Optimization for RF, Microwave, and Terahertz Applications, May 17-19, 2017, Sevilla, Spain.

D. Smacchia is with ESA-VSC High Power RF Space Laboratory, 46022, Valencia, Spain. Email: davide.smacchia@val-space.com

P. Soto, V. Boria, M. Guglielmi and J. Garnica are with iTEAM, Universitat Politècnica de València, 46022, Valencia, Spain. Email: pab-sopac@dcom.upv.es, vboria@dcom.upv.es, marco.guglielmi@iteam.upv.es

C. Carceller is with iTEAM, Universitat Politècnica de València. He is currently with Kyocera International Inc., San Diego, CA, 92111, USA.

J. Galdeano and D. Raboso are with European Space Research and Technology Centre, European Space Agency (ESTEC-ESA), Noordwijk, The Netherlands. Email: jaione.galdeano@esa.int, david.raboso@esa.int

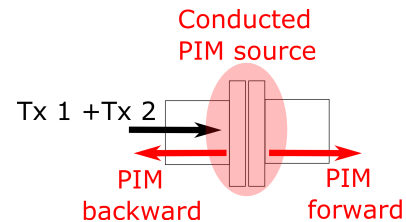


Fig. 1. Forward and backward PIM products from passive RF.

combining high power transmitted signals with weak received signals, which is usual in satellite communications, undesired PIM generation can, in fact, affect the throughput of the uplink or even cause, in extreme cases, the disruption of the whole reception channel.

PIM generation is normally attributed to thin oxide layers and non-ideal metal contacts. PIM sources on satellite payloads may be divided into two main categories: conducted and radiated [5]. Conducted PIM is related to non-ideal contacts between components in the downlink RF chain [5], [6]. For this kind of devices, PIM is generated both in the forward and in the backward direction, as shown in Fig. 1. Conducted PIM is typically measured in the forward direction [1], [7], [8]. However, different solutions for measuring backward PIM have also been discussed in the technical literature [7], [9]–[11].

Radiated PIM is instead generated by passive elements, such as reflecting meshes or multi-layer insulators (MLIs), illuminated by the downlink antennas. Typical measurement setups for radiated PIM make use of separate antennas to emit the high RF power signals and to collect the PIM generated (if any) [12]. However, reflected PIM test beds, using the same antenna to simultaneously transmit the high power carriers and receive the PIM signal, have also been reported [13].

The PIM specifications for high-power communication systems, such as direct broadcast satellites or military satellite systems, can be as low as -140 dBm. The measuring equipment must therefore be at least 5 or 10 dB better than the specified level of PIM. This is a tall order for standard measurement instrumentation. Invariably, it requires custom measurements setups, developed for specific measurement accuracy and system design [1], [14].

Classical satellite hardware test beds for measuring conducted or radiated PIM in the forward (transmitted) or backward (reflected) direction, are usually composed of the

cascaded connection of several blocks [5], [8], [12], [13]. This solution has several drawbacks. The interconnections degrade the return loss, are prone to generate unwanted spurious resonances, and also increase the number of flanged interconnections (which may become additional PIM sources). Moreover, the insertion loss of several individual elements is accumulated. Another classic limitation of such test benches is their low flexibility, as they are normally designed for only two particular input channels, and with a narrow detection bandwidth for measuring only one specific  $|m| \pm |n|$  PIM product term.

In this paper, novel high-performance PIM test beds for both conducted and radiated scenarios are described. The solutions that we propose are based on an integrated and compact structure, reducing the number of interconnected elements. In addition, the proposed test beds are flexible. They allow for the evaluation of several PIM orders without any modification of the setup, and can deal with more than two input carriers. The development of such integrated high-performance solutions introduces severe specifications for the hardware. Design aspects of the hardware and PIM measurements in various satellite bands are also included for completeness.

Due to the lack of detailed information on this topic, mainly to protect industrial know-how and proprietary information, it is difficult to assess the industrial state-of-the-art for PIM measurement setups for satellite hardware. The results provided in this paper can, therefore, also be useful to set a benchmark for PIM measurement test beds in various satellite frequency bands.

## II. PIM TEST SETUPS

### A. PIM setup design specifications

Typical customer requirements for PIM tests on elements of the RF chain of satellite payloads are compiled in Table I. As we can see, a PIM test bed must be able to handle very high power levels. Furthermore, low insertion losses are required to avoid unwanted thermal issues, and to conserve the power of the high power amplifiers (HPAs), the most expensive item in the measurement setup.

The test bed must also allow the detection of ultra-low PIM signals (about -150 dBm). This requirement implies that the PIM generated by the test bed itself must be extremely low to avoid masking the weak signal to be measured. As a result, low-PIM techniques must be used for the hardware design:

- Tuning elements must be avoided.
- The number of flanged interconnections must be minimized.
- The flanges must be designed to withstand high pressure in order to reduce (ideally avoid) PIM generation.
- The hardware assembly must not interrupt current lines, thus requiring single piece manufacturing (i.e., electroforming), or devices manufactured in two identical halves (clam shell manufacturing).

Furthermore, the huge dynamic range requirement (about 200 dB) imposes extremely high rejection levels. HPA in saturation can, in fact, provide spurious responses of about -50 dBc at frequencies that are  $\approx 10\%$  away from the carrier.

TABLE I  
TYPICAL CUSTOMER REQUIREMENTS FOR PIM TESTS

Tx 1	Tx 2	3rd order PIM	7th order PIM
52 (dBm)	52 (dBm)	$\leq -140$ dBm $\leq -192$ dBc	$\leq -150$ dBm $\leq -202$ dBc

As a consequence, the measurement hardware must ensure a rejection higher than 155 dB in the PIM reception band (see Table I). This specification can be normally relaxed for PIM bands placed far from the transmission band, as the spurious generated by HPAs decreases rapidly further away from the carrier.

One important consideration is that the low noise amplifier (LNA) connected to the PIM reception port of the test bed can produce significant levels (close to -150 dBm) of active intermodulation (AIM), when fed by two carriers with intensity greater than -80 dBm. This result is indeed confirmed by measurements. This AIM can overlap with the weak PIM signal to be detected, thus reducing the sensitivity of the test bed. To avoid this situation, the isolation of the PIM channel in the transmission band must be at least 140 dB (see Table I).

Last, but not least, the design of a custom test bed for each payload is impractical in terms of cost. As a result, flexible test beds need to be conceived.

### B. Conducted forward PIM

Let us start the discussion with test beds conceived for measuring conducted forward PIM. One solution for implementing flexible test beds consists of using a hybrid-based network to combine the input carriers [1], [5] (for reflected PIM, see for instance [11]). This solution provides high flexibility in terms of number of input carriers and their frequencies, but introduces the high insertion loss of the combining network (at least 3 dB for 2 carriers and 4.8 dB for 3 carriers). This approach is indeed possible for systems operating with moderate power levels (about 40-45 dBm), such as mobile networks [15]. However, power generation in satellite links operating at higher frequencies is very expensive, and a reduction of several decibels in input power cannot be tolerated.

For satellite applications, the most common solution consists of modular PIM test beds composed of several elements, which can be changed to fit each scenario. A typical diagram block is shown in Fig. 4 of [8], where a total number of 26 elements (including 7 filters and 2 diplexers) is used for only two input carriers. The input channels and the PIM reception channel are normally narrow band, so that a change in the input frequencies, or PIM order, normally requires a different set of filters and diplexers.

The innovative approach that we propose in this paper to detect conducted PIM in the forward direction is shown in Fig. 2.

This setup reduces the number of components of the test bed to the minimum: an input multiplexer that combines the input carriers, and a diplexer to separate the transmitted PIM signal from the input carriers. The input multiplexer is designed to be wideband with several input channels, thus allowing for the combination of two or even more input carriers in

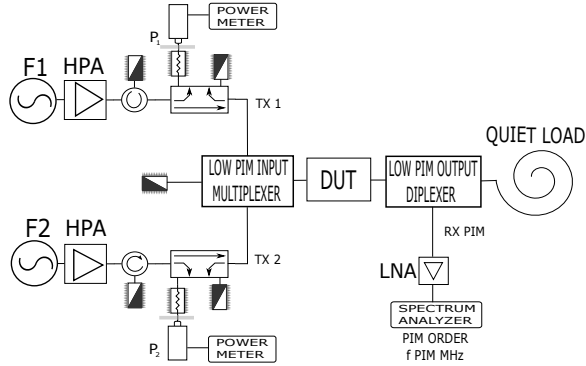


Fig. 2. Conducted PIM test bed for collecting forward PIM.

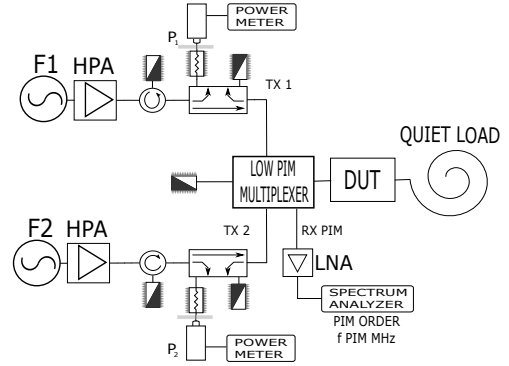


Fig. 3. Conducted PIM test bed for collecting backward PIM.

a wide frequency range. Similarly, the PIM detection channel of the output diplexer is also wideband. This allows for the measurement of several PIM orders with the same test bed. Note that the diplexer must also provide a moderate rejection (above 60 dB) in the PIM band between its output port (i.e., the one connected to the quiet load in Fig. 2) and its common and PIM reception ports. This rejection prevents the passive intermodulation generated by the input carriers at the quiet load (and its connection) from masking the weak signal to be detected in the PIM reception port.

This topology produces several benefits. First of all, a significant reduction of the number of mechanical connections in the main RF path. As a result, only the two connections to the device under test (DUT) can generate PIM (in contrast to the five connections in the diagram block of Fig. 4 in [8]). This helps to minimize the residual PIM level generated by the test bench. Other benefits introduced by this approach are its compactness, the lower insertion losses (due to the reduced number of filtering devices and flanged interconnections), as well as a considerable simplification of the test bed assembly.

In addition, since both the multiplexer and the diplexer integrate all the required filters in a single component, the proposed solution is not affected by unexpected response degradations. This represents a substantial improvement when compared with classical PIM setups [5], [8], [12], where the cascaded connections of several filters and diplexers can cause spurious resonance generation, and the deterioration of the overall return loss level (as it will be shown at the end of subsection III-A, and illustrated in Fig. 9).

It is also worth mentioning that this approach does not require low PIM specification for the load since the output diplexer blocks the interferences back-scattered from the load. A drawback from this setup is that special care must be dedicated to the output diplexer. This assembly must not add PIM to the measurements, and the reception filter must guarantee a 140 dB damping of the transmission carriers. Note, however, that if the transmission and PIM bands are separated enough, this point tends not to be critical.

### C. Conducted backward PIM

Following the same line of thought, the proposed solution to detect backward PIM is provided in Fig. 3.

As it can be noticed, the core of the test bench is composed by just one multiplexer, which integrates the transmission and reception filters in a single component. One of the channels of the multiplexer is dedicated to route the reflected PIM signal to the PIM reception port. The remaining channels are used to combine the different input carriers. Both the transmission and the PIM band are wideband, allowing for more than two input channels, if required. This increases very substantially the flexibility of the test bed. Furthermore, this setup has the same advantages already described in subsection II-B over classic backward PIM measurement setups composed of several cascaded elements [10], [11], [13]. The mechanical connections in the common RF path are again minimized, requiring only the DUT ports.

In addition, this configuration allows for the PIM measurement of one-port devices. Another advantage, if compared to the forward PIM scenario, is that collecting PIM in the backward direction allows for the relaxation of some of the filter specifications. In particular, the isolation between the transmission channels and the common port in the PIM reception band can be reduced by the return loss of the DUT. The same occurs to the rejection between the common port and the PIM port in the transmission band. Note that this reduction in the rejection levels, however, cannot be applied to the internal multiplexer isolation between its input ports and the PIM measurement port.

Backward PIM test benches are, however, very sensitive to imperfections in the common RF path, thus the utmost care must be devoted to the manufacturing of the multiplexer (symmetry and tolerances) and its common port. Moreover, as backward PIM setups are unprotected from degradations of the quiet load, the design of a low PIM and low noise load is fundamental to minimize the residual PIM signal generated by the test facility.

A compact single-piece backward PIM test (see Fig. 3) can extend up to a frequency range of about 30-40%, which is normally enough for low PIM orders (3rd, 5th or even 7th), that are the most critical ones in terms of amplitude and frequencies. On the other hand, this configuration may be unfeasible for PIM setups where the transmission and reception frequencies fall at quite separated bands. In such cases, the integration of the transmission and reception filters in the same manifold, without undesired harmful resonances,

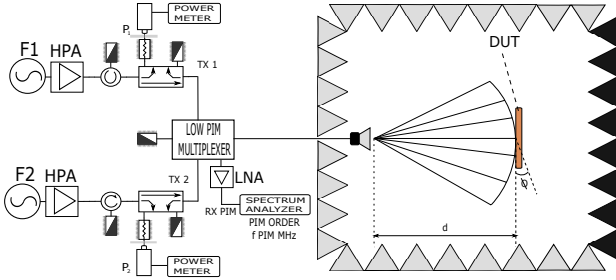


Fig. 4. Radiated PIM setup for detecting reflected PIM.

can be extremely complicated, even using special wideband techniques [16].

For separate transmission and reception bands, it is far better to use a forward PIM test bed. This simplifies the hardware design by separating the input combining multiplexer function from the output diplexer (at the cost of a bulkier and more expensive solution). Furthermore, for widely separated bands, the high-power tube-based HPAs tend to dramatically reduce the level of the spurious generated in the PIM bands. As a result, a rejection of only 60 dB of the input multiplexer at the PIM reception band may be enough to fulfill PIM specifications of about -200 dBc.

A further difference between backward and forward PIM measurements is related to how different PIM sources interact. According to research carried out with several identical coaxial connectors, PIM contributions add in-phase in the forward direction, whereas the phase difference (related to the different location of PIM sources) plays an important role in the backward PIM [17], [18]. Finally, further research is necessary in waveguide technology, specially for backward PIM measurement setups where the quiet load can be a significant source of PIM noise floor in addition to the flanged connections.

#### D. Radiated PIM

With a few modifications, a setup for evaluating conducted PIM in the backward direction may be also employed for radiated PIM measurements (see Fig. 4), thus inheriting all the advantages of integrated PIM test beds over traditional configurations [12], [13]. As it is shown in the figure, a horn antenna is connected to the multiplexer common port, which radiates towards the DUT located in a low-PIM anechoic chamber. The same antenna is used to receive the radiated PIM signal generated by the DUT.

A compact test bed for measuring radiated PIM could also be assembled using the elements of the forward PIM setup shown in Fig. 2, after connecting a transmitting and a receiving antenna to the common port of the multiplexer and diplexer, respectively [12]. However, the test setup for measuring reflected PIM has several practical advantages for satellite applications. First, the same antenna is used for both transmission and reception, so that the measurements are representative of the real PIM behavior of the DUT under operating conditions. Second, it allows for the measurement of PIM signal in foresight, which tends to be the worst case

scenario. Finally, the backward configuration eliminates the cross-coupling effects between antennas that might increase the noise floor of the setup (in the form of residual PIM generation or unwanted spurious/noise).

### III. HARDWARE IMPLEMENTATION

The compact PIM test beds proposed in section II provides several advantages over traditional setups, due to the integration of the different elements in a minimum number of hardware components. However, the complexity of the key components of the setup is clearly increased, as the requirements they must comply with are very demanding.

According to subsection II-A, multiplexers for PIM measurement setups must be low-loss, handle very high power levels, cover wide frequency ranges, include several channels, and guarantee outstanding rejection levels (about 140-160 dB) between transmission and reception bands without tuning elements. These are indeed demanding requirements, which must also be satisfied by all the filters included in the hardware.

Some techniques have been recently proposed for wideband multiplexing [16], reporting manufactured multiplexers with up to 6 channels and 40% relative bandwidth, suitable for PIM measurement test beds [16], [19]. However, the design issues related to the transmission and reception filters included in such multiplexing networks has not been described in depth. In this section, we will expand the work outlined in [20] including new detailed application examples.

#### A. Transmission filters

Two new families of low-loss high-power bandpass filters have been recently proposed, which are suitable for this particular application [19]. They are the Hybrid Folded Rectangular Waveguide (HFRW) filters [21], [22] and the Modified Hybrid Folded Rectangular Waveguide (MHFRW) filters [23].

The main practical differences between the two families lies in the number and position of the transmission zeros (TZs). The HFRW configuration can implement an independently controlled TZ for each cascaded trisection [16]. On the other hand, the MHFRW can generate one TZ for each coupling window (tuned by the stub created by the resonator location), thus allowing a higher number of TZs for the same filter order [23]. An advantage of the HFRW configuration is that the TZ can be placed very close to the filter passband [22]. For the MHFRW configuration, and in the cases where the coupling window must also provide a strong direct coupling, this is only possible for higher order resonators (i.e.,  $TE_{102}$  or above) [23].

After adding design margins, to cope with manufacturing tolerances and variations of the operating temperature, the first step for the design of the transmission filters is the choice of the resonator configuration. Particularly important is the selection of the resonant mode of the cavity ( $TE_{10p}$ ), due to its impact on the filter performance. Filters based on  $TE_{10p}$  resonators have a  $p$ -times stronger robustness against manufacturing tolerances than filters using  $TE_{101}$  resonators. This is a key point for the accurate implementation of tuning-less filters. In addition, power-handling capability and insertion losses are also improved. The disadvantages of using higher

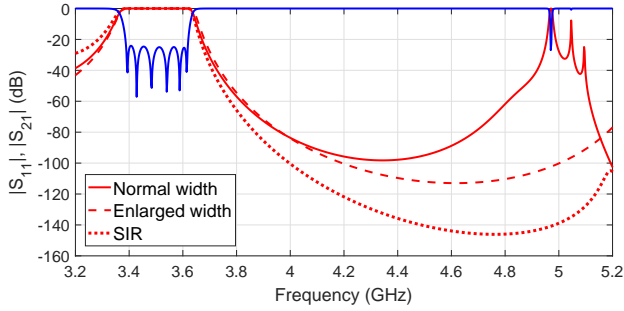


Fig. 5. Comparison between different resonator types for a 6th order HFRW filter with requested stopband ranging between 4.4 GHz and 4.9 GHz.

orders resonators for the filters are their larger size and relatively narrower spurious-free frequency window, due to the increased number of higher order modes coming into play in the frequency range of interest and also to the presence of lower order resonances in the response. This, in turn, limits the frequency range of the PIM test bed.

However, the spurious-free range and rejection of the receive band in the transmit filter can be improved by adjusting the resonator width, and by including capacitive sections in the HFRW or MHFRW resonators (i.e., using stepped-impedance resonators (SIR) [24]).

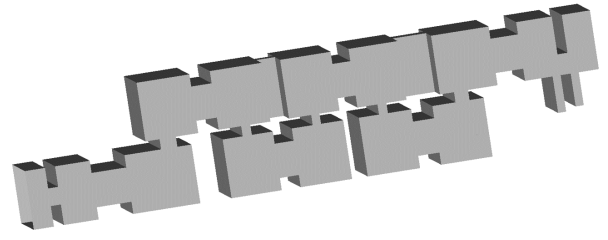
Fig. 5 shows the stopband performance of a 6th order HFRW filter with  $TE_{101}$  resonators that must provide a high rejection in the frequency range between 4.4 GHz and 4.9 GHz. The design with the same width as the input port (WR229 standard), is not suitable for such an application due to the spurious passband at about 5 GHz. A filter with enlarged width is able to shift this undesired passband to higher frequencies (although special attention must be devoted to the response of higher order modes which can be excited by manufacturing or assembling asymmetries, such as the  $TE_{20}$ ). The best performance in rejection terms is obtained using a stepped-impedance resonator (SIR) configuration maintaining the original width, at the expense of the higher insertion losses related to the capacitive sections inside the resonators.

Once the resonator shape has been chosen, the maximum order of the filter for tuning-less implementation must be determined.

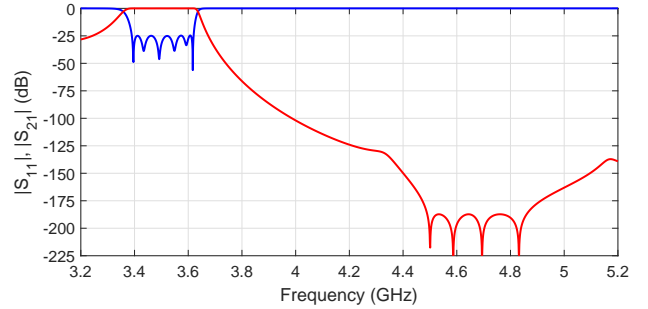
Although, as reported in [25], the required manufacturing tolerance  $T$  is found to be proportional to the relative bandwidth and inversely proportional to filter order and center frequency, we prefer to use the following improved expression [26]:

$$T \propto p \frac{BW_r \lambda_{g,wg}^{1.5}}{N^{1.5} \lambda_{g,0}^{0.5}} \quad (1)$$

where  $BW_r$  is the relative bandwidth in wavelength terms,  $N$  is the filter order,  $p$  is the resonance order of the cavity ( $TE_{10p}$  mode),  $\lambda_{g,0}$  is the guided wavelength at the passband center frequency and  $\lambda_{g,wg}$  is the wavelength at the center frequency of the recommended operational band of the waveguide. It is important to appreciate that the minimum manufacturing tolerance depends on the manufacturer capabilities, determines the fabrication cost, the filter manufacturing processes and



(a)



(b)

Fig. 6. (a) Topology of a 6th order HFRW filter with SIR resonators providing 4 transmission zeros. (b) Optimized final response.

materials, and it imposes a limit to the possible maximum filter order.

Furthermore, although the expression in equation (1) has been proven in practice to be quite accurate, the initial guess provided for the filter order must always be verified by means of a Montecarlo analysis carried out on the design parameters and more sensitive filter dimensions. This check can be performed using an initial HFRW or MHFRW structure without transmission zeros, and later confirmed for the final topology including all the needed TZs.

At this point, the designer must choose between a HFRW or MHFRW topology. This choice essentially depends on the separation between transmission and PIM bands, since MHFRW filters may not be able to implement the TZs at the requested PIM reception band if the two frequency bands are too close to each other.

The following step is the choice of the filter layout, as it will be later integrated in a multiplexer. Heat dissipation, proper mechanical coupling between filter halves (which requires additional space for placing screws), multiplexer compactness, and appropriate location of the waveguide ports to ease the external connections are all important issues that must be taken into account. The final physical arrangement of the filter can also reduce the maximum number of attainable TZs, especially for the HFRW topology. In addition, to increase the isolation between the filters attached to the multiplexer (avoiding unwanted resonances due to the filter interconnection network [16]), the first TZ of the filter should not be introduced before the end of the first resonator. If a higher rejection is required in the PIM reception band, the designer can replace some filter coupling windows with the capacitive obstacle proposed in [27], which is able to provide additional transmission zeros.

If the HFRW or MHFRW filter designed is unable to provide

the extremely high rejection required between the transmission band and the PIM reception band (see subsection II-A), a low-pass filter or a high-pass filter (depending on the frequency position of the PIM reception band with respect to the transmission channels) can be attached. An integrated design is preferred, since it is able to avoid noticeable return loss degradation, can shift the spurious resonances due to the filter interconnection outside of the PIM reception band, and improve manufacturing robustness against tolerances.

The first example of transmission filter for a PIM setup is shown in Fig. 6. It corresponds to the first channel of the C-Band PIM setup reported in [16]. The transmission band ranges between 3.4 GHz and 4.26 GHz, whereas the reception PIM band is located between 4.5 GHz and 4.85 GHz. The wide bandwidth involved (36%) only allowed  $TE_{101}$  resonant cavities to be used. An HFRW filter topology was chosen for all the transmission channels, due to the proximity between the transmission and reception bands. The first channel was designed to provide a passband between 3.39 GHz and 3.62 GHz with a return loss of 25 dB. A stepped-impedance resonator was used to improve the rejection in the relatively far PIM reception band (see Fig. 5).

With the tolerances available at the time of manufacturing, the maximum filter order was 6, in order to ensure a passband return loss greater than 20 dB. This filter order allows the introduction of 2 HFRW cascaded trisections, thus providing 2 TZs. The attenuation obtained with these 2 TZs in the PIM band was lower than the goal rejection of 165 dB. Therefore, an output coupling window providing 2 extra TZs was included in the final design [27], as shown in Fig. 6a. Fig. 6b represents the final response of the filter designed using AuroraSAT FEST3D v6.9.

The second illustrative example is a transmission filter for a K/Ka-band PIM measurement setup, as shown in Fig. 7. The required filter passband ranges between 21 GHz and 22 GHz, whereas the PIM reception band extends from 27 GHz to 31 GHz. Again, only  $TE_{101}$  cavities are able to avoid undesired spurious passband in the wide PIM reception band. A MHFRW filter topology was selected, since the PIM reception band is far enough from the filter passband. The maximum filter order allowed by the manufacturing tolerance was only 4 for a return loss goal of 20 dB.

The MHFRW filter topology has the capability of providing a high number of TZs, as shown in Fig. 7 and 8. In this case, 5 independent TZs were implemented in a 4th order filter. The number of attainable TZs is higher than the filter order since the TZ generation is not limited to the well-known cross-coupled configurations [1]. In this implementation, two of the TZs are provided by the coupling window between first and second resonator [27]. The other 3 TZs are generated in the following coupling windows of the structure, being controlled by the stub sections highlighted in Fig. 7 [23]. The reported topology also exhibits geometrical flexibility. The bandpass filter shape has, in fact, been optimized to reduce the multiplexer footprint, and to have the best port positioning to facilitate the external connections of the test bed.

Due to the huge bandwidth of the PIM reception band, the rejection provided by the MHFRW filter on its own did not

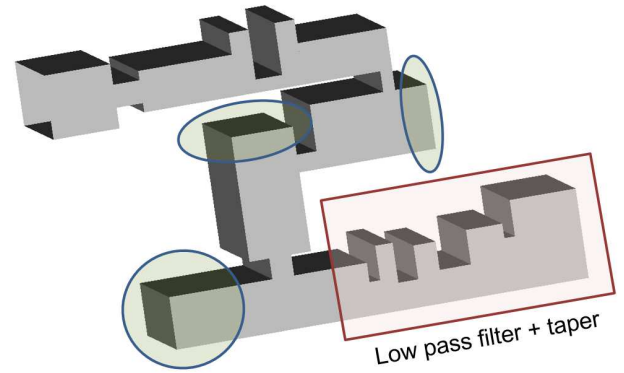


Fig. 7. Final topology of a transmission filter composed of a 4th order MHFRW bandpass filter with an integrated low-pass filter. The bandpass filter provides 5 transmission zeros, 3 of them controlled by the stubs remarked with ovals.

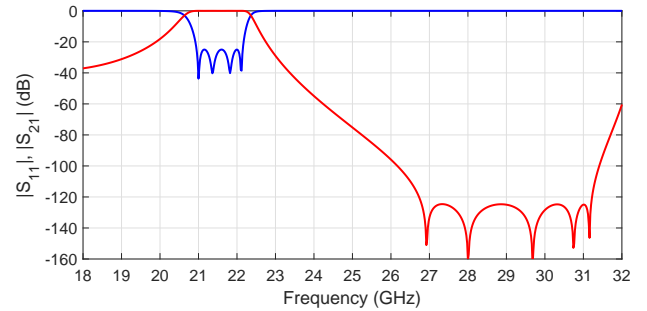


Fig. 8. Optimized response of the isolated 4th order MHFRW bandpass filter with 5 transmission zeros.

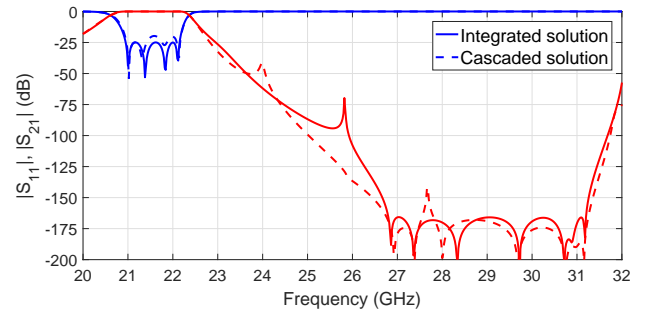


Fig. 9. Comparison between an integrated design of the bandpass and low-pass filters, and a cascaded connection of both filters through a waveguide section of 15 mm.

fulfill the rejection requirements for this particular application. A low-pass filter has therefore been added in the transmission channel (see Fig. 7). In contrast to classical PIM test beds, the low-pass filter must not be an external element to be connected in cascade to the input channel bandpass filter. In our solution, an integrated design of both elements has been carried out resulting into a more compact hardware.

There are important differences in the performance of each solution, as shown in Fig. 9. The cascaded solution is formed by connecting a 25 dB return loss low-pass filter to the MHFRW filter (see its isolated response in Fig. 8) through a 15 mm length waveguide section. The return loss of the cascaded configuration is degraded by about 5 dB (theoretically, it can

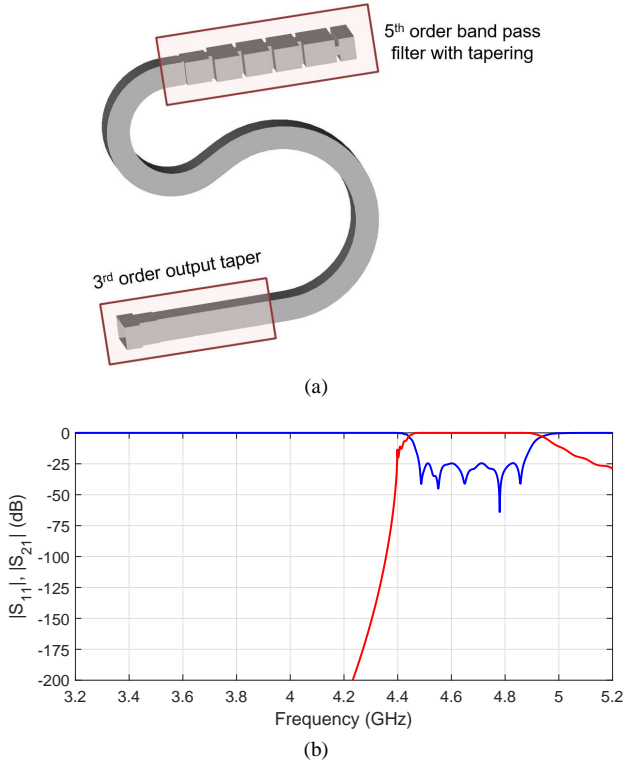


Fig. 10. (a) Topology of the PIM reception filter for on-board hardware composed of a band-pass filter and a high-pass section. (b) Optimized final response.

reach up to 6 dB), and an unwanted resonance appears in the PIM band (since both filters are reflective at the PIM reception band, the interconnecting waveguide creates a highly selective resonator). In the integrated design, the return loss degradation can be compensated, and the spurious resonance can be controlled and shifted to non-harmful frequencies. It is worth pointing out that a PIM measurement setup composed of separated elements connected in cascade would have accumulated several degradations of this kind. In the diagram block in Fig. 4 in [8], up to three filters and a diplexer are connected in cascade for each input channel, thus implying a severe impact in the overall PIM test bed performance. This is one of the key advantages of the novel integrated PIM test beds proposed in section II.

### B. Reception filters

For a flexible PIM test bed enabling the measurement of different PIM order terms, the bandwidth of the PIM band is normally wider than the one of an isolated input channel. Higher filter orders can therefore be used. In addition, the typical rejection levels needed are somewhat lower (see subsection II-A) and are required on one side of the passband only. As a result, the design of PIM reception filters is normally easier than the design of transmission filters.

In applications where the PIM reception band is placed at frequencies that are higher than the transmission band (the usual situation of satellite payloads), the proposed solution is a bandpass filter followed by a high-pass section. The band pass filter performs three important tasks, namely, its resonators

isolate the reception filter from the rest of filters integrated in the wideband multiplexer/diplexer (avoiding unwanted resonances), performs the tapering to the high-pass section, and simultaneously increases the rejection of the input carriers.

A practical example is shown in Fig. 10a, where a 5th order direct-coupled band pass filter is followed by a high-pass section. Note that this filter also performs the tapering and contributes to about a third part of the attained rejection in the transmission band. The response of the complete PIM reception filter is shown in Fig. 10b, and fulfills the rejection needs in the transmission band. Note also the slightly irregular shape of the 25 dB passband ripple, due to interactions between the bandpass and the high pass filters which can be kept under control in an integrated design.

If, on the other hand, the PIM reception band is placed below the transmission channels, the usual solution is a stub-based low-pass filter with enhanced rejection in the transmission band [28]. The low-pass filter normally outperforms a passband filter (provided that enough separation exists between the PIM and transmission bands) thanks to the non-resonant nature of its elements. It normally takes up less physical space, with smaller insertion losses and shows improved robustness to manufacturing tolerances.

## IV. EXPERIMENTAL RESULTS

Several PIM measurement setups have been developed following the theory and guidelines described in this paper (see Sections II and III). Some of the multiplexers developed have been discussed in the technical literature as application examples of wideband design and multiplexing techniques [16], [19]. In this section, we will focus on the passive intermodulation performance of the test beds by describing the excellent results obtained in several conducted and radiated test campaigns.

### A. Conducted forward PIM test bench

A measurement setup for conducted PIM in forward direction in K/Ka-band, as sketched in Fig. 2, has been designed, fabricated and mounted. A photograph of the resulting PIM test bed is shown in Fig. 11.

This test bench operates at K/Ka-bands following the ITU Regulations for Ka-band satellite Payloads [29]. The core of the setup is composed by an input triplexer able to combine up to three high-power input carriers in K-band (17.3 GHz to 22 GHz) and one output diplexer whose reception channel is designed to operate in Ka-band (27 GHz to 31 GHz). Depending on the combination of transmission carriers, several PIM orders can be collected at the PIM reception port (5th, 7th, 9th, 11th, 13th, etc...). The insertion loss was about 0.5 dB in the worst input channel, clearly showing the superior insertion loss performance of this integrated solution. The huge bandwidth covered by this setup made unsuitable an integrated solution for backward conducted PIM, as the one shown in Fig. 3.

The measurement technique employed to calibrate both the transmission carriers and the PIM noise floor is based on a standard procedure of the ESA-VSC labs, which is consistent

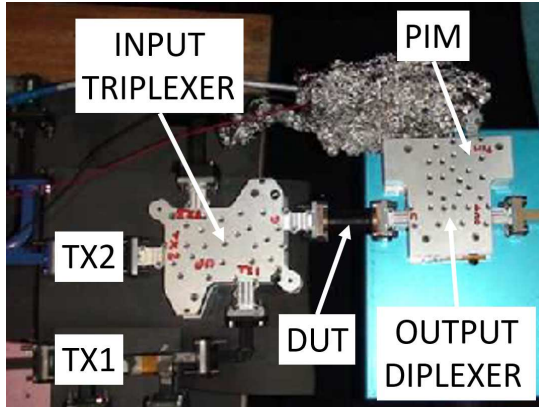


Fig. 11. K/Ka-band setup assembled for collecting forward conducted PIM.

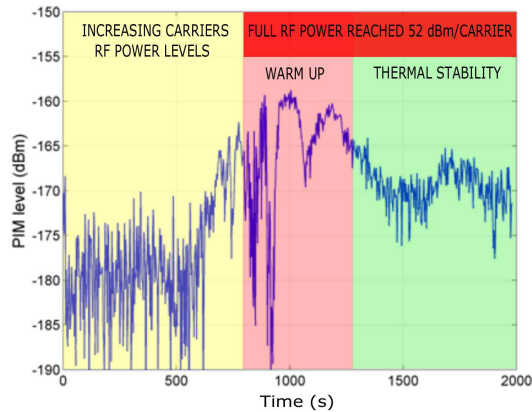


Fig. 12. Evolution of 7th order PIM level versus time for the K/Ka-band PIM setup with two input carriers of 160 W.

TABLE II  
CONDUCTED FORWARD PIM AT K/KA-BANDS, TEST RESULTS.

	Tx 1	Tx 2	7th order PIM
<b>Frequency (GHz)</b>	17.5	20.0	27.5
<b>RF levels (dBm)</b>	52	52	$\leq -165$ (*)

(\*) After thermal stabilization

with the one already described in [1]. This procedure can be summarized as follows.

Referring to Fig. 2, both the transmission carriers and the PIM level were calibrated at the input port of the output diplexer (DUT reference plane). The calibration for each transmission channel consisted in measuring the offset between the reference plane and the power meter, at the corresponding transmission frequency signal. The PIM channel was calibrated by injecting a weak carrier at the PIM frequency (about -90 dBm) through the input port of the output diplexer. The amplified signal displayed by the spectrum analyzer provided an offset to be subtracted from the actual PIM measurement. Once the power level at the reference plane has been defined, the next step was to validate the test facility without the DUT, in order to provide the value of the residual PIM noise floor of the setup. The last step was to check the effective capability of the test setup to detect a weak PIM signal, by inserting as DUT a sample having well known poor PIM performance.

The validation results are provided in Table II, where a straight WR51 waveguide section, manufactured in a single piece, was inserted between the input triplexer and the output diplexer in order to consent the physical mating between the two components. This short low-PIM waveguide section will therefore be assumed as part of the setup. Two input RF carriers of 160 W each were injected in the setup, and a 7th order PIM product was measured. Fig. 12 shows the evolution of the PIM signal detected in terms of time. Once the power of both carriers reached 160 W, a transmitted PIM level of -160 dBm was measured. However, after waiting the thermal stabilization of the setup, the detected PIM level decreased to the range between -165 and -168 dBm. Therefore, the residual PIM level of the measurement test bed, probably due to the high-pressure input and output flanged connections to the common RF path, was around -165 dBm (see Table II). Observe the difference in complexity between this forward PIM test bed and the ones reported in [5], [8], as well as the reduction in the number of interconnections capable of generating undesired PIM.

Next, the DUT was replaced with a short section of WR51 flexible waveguide, and a PIM signal of -113 dBm was detected in the spectrum analyzer.

These results prove the validity of the proposed PIM measurement setup, and the excellent residual PIM level of the complete test facility. Unfortunately, to the authors knowledge, there is not published data of noise floor for PIM measurement setups working at K/Ka band. Anyway, a comparison with the data from forward PIM test beds at Ku-band reported in Table 20.7 in [1] (noise floor of -140 dBm for 3rd order PIM with two 46 dBm input carriers) and in [8] (noise floor of about -145 dBm for 3rd order PIM with two 52 dBm input carriers) shows the excellent performance of this setup operating at a higher frequency range. Note also that the thermal noise limit for the 1 Hz detection bandwidth used in the measurements is about -173 dBm.

### B. Conducted backward PIM test benches

In order to perform backward conducted PIM measurements, a test bench operating at C-band was assembled as described in Fig. 3. The test bench operates at C-band covering almost the whole WR229 recommended operational frequency range. This is close to the maximum achievable bandwidth for a test bed composed of a single multiplexer combining the input carriers, and separating the reflected PIM signal.

The core of the setup is a four channel multiplexer able to combine up to three RF carriers in the frequency band between 3.4 GHz and 4.26 GHz, and one reception filter with passband between 4.5 GHz and 4.85 GHz. Depending on the transmission carriers, several odd PIM orders can be collected at the PIM reception port (3th, 5th, 7th and 9th). The overall insertion loss was again below 0.5 dB for all the input channels.

The same calibration procedure described in subsection IV-A was applied, considering as DUT reference plane the common port of the multiplexer.

Table III summarizes the results from a PIM measurement, where two input RF carriers were employed to evaluate the

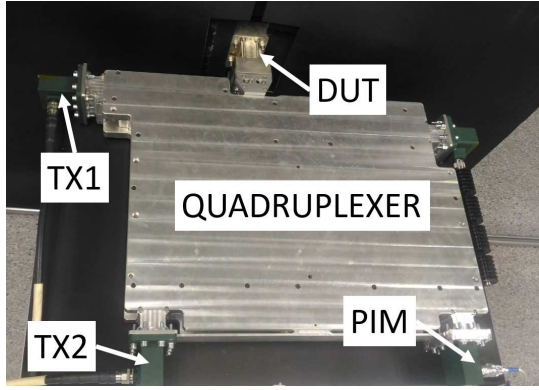


Fig. 13. C-band setup assembled for testing backward conducted PIM.

TABLE III  
CONDUCTED BACKWARD PIM AT C-BAND, TEST RESULTS.

	Tx 1	Tx 2	3rd order PIM
Frequency (GHz)	3.58	4.17	4.76
RF levels (dBm)	50	50	$\leq -137$

TABLE IV  
CONDUCTED BACKWARD PIM AT KU-BAND, TEST RESULTS.

	Tx 1	Tx 2	3rd order PIM
Frequency (GHz)	11.468	12.735	14.002
RF levels (dBm)	52	52	$\leq -145$

3rd PIM order of a straight WR229 standard waveguide (see Fig. 13). The measured PIM level could be attributed to the quiet load rather than the multiplexer itself. The results implies a margin greater than 15 dB with respect to typical PIM specification at C band, as reported in the last sentence of section 1.8.4 of [1], thus confirming the effectiveness of the system to evaluate the PIM performance of satellite hardware.

This C-band quadruplexer has also been successfully used in a test campaign to measure the PIM generated by three input carriers operating simultaneously, and for thermal tests combining more than 2000 W at the DUT port. These results clearly demonstrate the flexibility of this PIM test bed designed to cover the whole C-band frequency range.

Another test bed for evaluating the conducted PIM performance in the backward direction for Ku-band has also been developed. This test bed has been designed to fit the specifications of the ESA Small Geo Payload. It was assembled and used to evaluate the PIM performance of the Compact Antenna Test Range (CATR) facility in which the payload was tested before launching the satellite.

The main element of this PIM setup is a three port multiplexer with two moderate bandwidth transmission channels, in the band from 11.15 GHz to 12.75 GHz, and with a PIM channel working in the frequency range between 13.7 GHz and 14.55 GHz. Depending on the particular frequency of the transmission carriers, 3rd, 5th and 7th order PIM terms could be collected at the PIM reception port.

Taking the common port of the multiplexer as the DUT reference port, and after applying the calibration procedure described in subsection IV-A, the setup was first operated

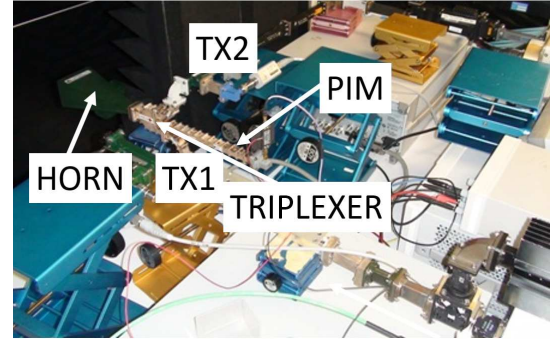


Fig. 14. Ku-band setup assembled for testing radiated PIM.

TABLE V  
RADIATED PIM AT KU-BAND, TEST RESULTS.

	Tx 1	Tx 2	3rd order PIM
Frequency (GHz)	11.468	12.735	14.002
RF levels (dBm)	52	52	$\leq -145$ with Blank
	50	50	$\leq -132$ with MLI

with a straight piece of waveguide (spacer) as DUT. The measured results for 3rd order PIM with two input carriers of 160 W at the DUT port are compiled in Table IV. The same setup was employed to evaluate higher PIM orders (5th, 7th), showing a noise floor below -152 dBm in both cases. The results obtained for 3rd order PIM are essentially the same as the state-of-art PIM measurement setup for conducted forward PIM at Ku-band used in [8], although backward PIM measurement setups may be noisier as they are affected by the PIM generated at the quiet load. Anyway, the proposed integrated setup has advantages in terms of flexibility, compactness, ease of assembly, insertion loss, return loss degradation, and spurious generation from PIM measurement setups based on the cascaded connection of several blocks.

### C. Radiated test benches for measuring reflected PIM

The same Ku-band test bench used for backward conducted PIM measurements just described, was modified by the insertion of a horn antenna in the common RF port of the multiplexer (see equivalent block diagram in Fig. 4). As a result, a test bed to perform radiated PIM tests was obtained, as shown in Fig. 14. Measurements were carried out with the antenna placed inside a sealed anechoic chamber, in order to dissipate the radiated power from the carriers and minimize the disturbances from the environment, which may mask the effective PIM signal to be measured.

The performance of the facility was evaluated for third order PIM with two test scenarios, the blank one (radiation through the anechoic chamber walls) and after inserting a multi layer insulator (MLI) sample at 1.2 m from the horn as DUT. The measured results are summarized in Table V. As it can be observed, a low-PIM high performance multiplexer conceived for measuring conducted backward PIM is also suitable to perform accurate measurements on reflected radiated PIM signals.

## V. CONCLUSION

In this paper, novel, compact and flexible PIM measurement test beds for satellite systems are described. Instead of the traditional solution based on the cascaded connection of several devices, an integrated and high-performance solution based on manifold multiplexers is proposed. The number of flanged interconnections is therefore reduced to a minimum. This results in lower PIM generation by the test bed, reduced insertion losses, absence of return loss degradation, and avoidance of harmful spurious resonances related to component interconnections.

The PIM measurement setups discussed cover wide frequency ranges and are not limited to only two input channels. As a result, several orders of PIM generated with different number of carriers placed at different frequencies can be measured effectively with the same test bed.

An integrated solution, however, results in extremely demanding specifications for the wideband multiplexers and filters for the test bed. Key guidelines and examples for the development of such filters and multiplexers are included in the paper.

Experimental results from different test campaigns, carried out with PIM measurement test beds developed according to the principles proposed in this paper, are described. The measured values of PIM over different frequency bands clearly demonstrate the flexibility and accuracy (close to fundamental limit set by thermal noise) of the test equipment.

Finally, we believe that the PIM measurement test beds presented in this paper, and the experimental results obtained, represent a benchmark for PIM measurements in satellite systems.

## ACKNOWLEDGMENT

The authors would like to thank the European Space Agency (ESA), the Val Space Consortium (VSC) and the ESA-VSC High Power RF Space Laboratory (A laboratory funded by the European Regional Development Fund – A way of making Europe) for their support to this work. The authors would also like to thank to the unknown reviewers whose comments have indeed contributed to improve the final version of this paper.

## REFERENCES

- [1] R. J. Cameron, C. M. Kudsia, and R. R. Mansour, *Microwave Filters for Communication Systems: Fundamentals, Design and Applications*. New Jersey: John Wiley & Sons, 2007, sections 18.4 and 20.7.
- [2] Y. Ming and A. Atia (organizers), "High power issues of microwave filter design and realization," in *2007 IEEE MTT-S Workshop Proc.*, Honolulu, Hawaii, June 2007.
- [3] J. W. Boyhan and H. F. Lenzing, "Satellite passive intermodulation: system considerations," *IEEE Trans. Aerosp. Electron. Syst.*, vol. 32, no. 3, pp. 1058–1064, July 1996.
- [4] F. Carducci, "Passive intermodulations aspects on ITALSAT F2/EMS spacecraft," in *Proc. of Int. Symp. on Antenna Technology and Applied Electromagnetics*, Aug. 1994, pp. 377–380.
- [5] P. Lui, "Passive intermodulation interference in communication systems," *Electronics and Communication Engineering Journal*, vol. 2, no. 3, pp. 109–118, June 1990.
- [6] C. Vicente and H. L. Hartnagel, "Passive-intermodulation analysis between rough rectangular waveguide flanges," *IEEE Trans. Microw. Theory Techn.*, vol. 53, no. 8, pp. 2515–2525, Aug. 2005.
- [7] B. Rosenberger, "The measurement of intermodulation products on passive components and transmission lines," in *Proc. of 50th ARFTG Conference Digest*, Dec. 1997, pp. 13–22.
- [8] C. Vicente, D. Wolk, H. L. Hartnagel, B. Gimeno, V. E. Boria, and D. Raboso, "Experimental analysis of passive intermodulation at waveguide flange bolted connections," *IEEE Trans. Microw. Theory Techn.*, vol. 55, no. 5, pp. 1018–1028, May 2007.
- [9] M. Bayrak and F. A. Benson, "Intermodulation products from nonlinearities in transmission lines at connectors at microwave frequencies," *Proc. IEEE*, vol. 122, no. 4, pp. 361–367, Apr. 1975.
- [10] F. Arazm and F. A. Benson, "Nonlinearities in metal contacts at microwave frequencies," *IEEE Trans. Electromagn. Compat.*, vol. 22, no. 3, pp. 142–149, Aug. 1980.
- [11] A. J. Christianson, J. J. Henrie, and W. J. Chappell, "Higher order intermodulation product measurement of passive components," *IEEE Trans. Microw. Theory Techn.*, vol. 56, no. 7, pp. 1729–1736, July 2008.
- [12] S. Rao and L. Shafai, *Handbook of Reflector Antennas and Feed Systems (Volume 3)*. Boston, USA: Artech House, 2013.
- [13] P. Bolli, S. Selleri, and G. Pelosi, "Passive intermodulation on large reflector antennas," *IEEE Antennas Propag. Mag.*, vol. 4, no. 5, pp. 13–20, Oct. 2002.
- [14] S. Mishra and Y. Patenaude, "A review of recent advances in passive intermodulation and multipaction measurement techniques," in *Proc. of 12th Int. Symp. on Antenna Technology and Applied Electromagnetics*, July 2006, pp. 1–4.
- [15] *Passive RF and Microwave Devices Intermodulation Level Measurement*, International Electrotechnical Commission (IEC) Std. 62 037, 2012.
- [16] C. Carceller, P. Soto, V. E. Boria, M. Guglielmi, and J. Gil, "Design of compact wideband manifold-coupled multiplexers," *IEEE Trans. Microw. Theory Techn.*, vol. 63, no. 10, pp. 3398–3407, Oct. 2015.
- [17] B. Deats and R. Hartman, "Measuring the passive-IM performance of RF cable assemblies," *Microw. RF Eng.*, vol. 36, pp. 108–114, Mar. 1997.
- [18] J. Henrie, A. Christianson, and W. J. Chappell, "Prediction of passive intermodulation from coaxial connectors in microwave networks," *IEEE Trans. Microw. Theory Techn.*, vol. 56, no. 1, pp. 209–216, Jan 2008.
- [19] P. Soto, D. Smacchia, C. Carceller, V. E. Boria, and M. Guglielmi, "Computer-aided design (CAD) of filters and multiplexers for passive inter-modulation (PIM) set-ups," in *Proc. of 2016 IEEE MTT-S Latin America Microwave Conference*, May 2016, pp. 1–3.
- [20] P. Soto et al., "Design of advanced waveguide filters for passive intermodulation measurement setups," in *Proc. of 2017 IEEE MTT-S Int. Conf. on Numerical Electromagnetic and Multiphysics Modeling and Optimization for RF, Microwave, and Terahertz Applications*, May 2017, pp. 335–337.
- [21] M. Guglielmi, "Hybrid folded rectangular waveguide filter," European Space Agency Patent PCT/EP2013/072 406, 2013.
- [22] C. Carceller, P. Soto, V. E. Boria, and M. Guglielmi, "Design of hybrid folded rectangular waveguide filters with transmission zeros below the passband," *IEEE Trans. Microw. Theory Techn.*, vol. 64, no. 2, pp. 475–485, Feb. 2016.
- [23] P. Soto, V. E. Boria, C. Carceller, S. Cogollos, M. Guglielmi, and D. Smacchia, "Practical design of rectangular waveguide filters with a capacitive building block providing an extra transmission zero," in *Proc. of 2015 IEEE MTT-S Int. Microw. Conf.*, May 2015, pp. 1–4.
- [24] M. Morelli, I. Hunter, R. Parry, and V. Postoyalko, "Stopband performance improvement of rectangular waveguide filters using stepped-impedance resonators," *IEEE Trans. Microw. Theory Techn.*, vol. 50, no. 7, pp. 1657–1664, July 2002.
- [25] M. Guglielmi and G. Connor, "Industrial implementation of tuning-less microwave filters," *Microwave Eng. Europe*, pp. 39–40, 1996.
- [26] P. Soto, V. E. Boria, C. Carceller, C. P. Vicente, J. Gil, and B. Gimeno, "EM-based synthesis and design of bandpass waveguide filters including manufacturing effects with FEST3D," *Int. J. RF Microw. Comput. Aided Eng.*, vol. 22, no. 1, pp. 93–103, Jan. 2012.
- [27] C. Carceller, P. Soto, V. E. Boria, and M. Guglielmi, "Capacitive obstacle realizing multiple transmission zeros for in-line rectangular waveguide filters," *IEEE Microw. Wireless Compon. Lett.*, vol. 26, no. 10, pp. 795–797, Oct. 2016.
- [28] J. Uher, J. Bornemann, and U. Rosenberg, *Waveguide Components for Antenna Feed Systems: Theory and CAD*. Norwood, MA: Artech House, 1993.
- [29] A. J. Christensen, "ITU regulations for Ka-band satellite networks," in *30th AIAA International Communications Satellite System Conference (ICSSC)*, Sept 2012, pp. 524–527.



**Davide Smacchia** was born in 1982 in Fano, Italy. He received the M.S. degree (cum Laude) in Electronic Engineering from the Università di Perugia in 2008. He is currently working towards the Ph.D. degree.

From 2008 to 2010 he was a researcher at Departamento de Comunicaciones, Universidad Politécnica de Valencia, Valencia, Spain, granted by a Generalitat Valenciana Grisolia fellowship. In 2010 he joined the ESA-VSC High Power RF Space Laboratory, Valencia, Spain. His research interests comprise RF breakdown phenomena, such as multipactor and corona, as well as the analysis and measurement of passive intermodulation (PIM) for both conducted and radiated scenarios.



**Pablo Soto** (S'01-M'06) was born in 1975 in Cartagena, Spain. He received the M.S. degree and Ph.D. degree (cum Laude) in Telecommunication Engineering from the Universidad Politécnica de Valencia in 1999 and 2012, respectively.

In 2000, he joined the Departamento de Comunicaciones, Universidad Politécnica de Valencia, where he is Associate Professor since 2012. He was an EU research fellow with the European Space Research and Technology Centre (ESTEC-ESA), Noordwijk, the Netherlands in 2000. His research interests comprise numerical methods for the analysis, synthesis, and fully automated design of passive components in waveguide and planar technologies, the development and design of novel hardware for satellite applications, and high power RF effects.

Dr. Soto received the 2000 and 2012 COIT/AEIT national awards to the best Master Thesis and best Ph.D. Thesis in Basic Information and Communication Technologies, respectively. He is also the co-recipient of the 2013 Gheorghe Cartianu Award of the Academia Romana.



**Vicente E. Boria** (S'91-A'99-SM'02-F'18) was born in Valencia, Spain, on May 18, 1970. He received his Ingeniero de Telecomunicación degree (with first-class honors) and the Doctor Ingeniero de Telecomunicación degree from the Universidad Politécnica de Valencia, Valencia, Spain, in 1993 and 1997, respectively.

In 1993 he joined the Departamento de Comunicaciones, Universidad Politécnica de Valencia, where he has been Full Professor since 2003. In 1995 and 1996, he was holding a Spanish Trainee position

with the European Space Research and Technology Centre, European Space Agency (ESTEC-ESA), Noordwijk, The Netherlands, where he was involved in the area of EM analysis and design of passive waveguide devices. He has authored or co-authored 10 chapters in technical textbooks, 160 papers in refereed international technical journals, and over 200 papers in international conference proceedings. His current research interests are focused on the analysis and automated design of passive components, left-handed and periodic structures, as well as on the simulation and measurement of power effects in passive waveguide systems.

Dr. Boria has been a member of the IEEE Microwave Theory and Techniques Society (IEEE MTT-S) and the IEEE Antennas and Propagation Society (IEEE AP-S) since 1992. He is member of the Editorial Boards of the IEEE Transactions on Microwave Theory and Techniques, IEEE Microwave and Wireless Components Letters, Proceeding of the IET (Microwaves, Antennas and Propagation), IET Electronics Letters and Radio Science. Presently, he serves as Associate Editor of IEEE Microwave and Wireless Components Letters and IET Electronics Letters. He is also a member of the Technical Committees of the IEEE-MTT International Microwave Symposium and of the European Microwave Conference.



**Marco Guglielmi** (S'79-M'81-SM'97-F'13) was born in Rome, Italy, on December 17, 1954. He received the degree Laurea in Ingegneria Elettronica in 1979 from the University of Rome La Sapienza, Rome, Italy, where in 1980 he also attended the Scuola di Specializzazione in Elettromagnetismo Applicato. In 1981 he was awarded a Fulbright Scholarship in Rome, Italy, and an HISP (Halsey International Scholarship Programme) from the University of Bridgeport, Bridgeport, Connecticut, USA, where in 1982 he obtained an M.S. Degree in Electrical Engineering. In 1986 he received a Ph.D. degree in Electrophysics from the Polytechnic University, Brooklyn, New York, USA.

From 1984 to 1986 he was Academic Associate at Polytechnic University, and from 1986 to 1988 he was Assistant Professor in the same institution. From 1988 to 1989 he was Assistant Professor at the New Jersey Institute of Technology, Newark, New Jersey, USA. In 1989 he joined the European Space Agency as a Senior Microwave Engineer in the RF System Division of the European Space Research and Technology Centre (ESTEC), Noordwijk, The Netherlands, where he was in charge of the development of microwave filters and electromagnetic simulation tools. In 2001 he was appointed Head of the Technology Strategy Section of ESTEC where he contributed to the development of management processes and tools for the formulation of a European strategy for space technology research and development.

In 2014 Dr. Guglielmi retired from the European Space Agency and is currently holding the position of Invited Senior Researcher at the Polytechnic University of Valencia, Valencia, Spain. Dr. Guglielmi has been elevated to the grade of Fellow of the IEEE in January 2013 "For contributions to multimode equivalent networks and microwave filter design".



**Carlos Carceller** (S'06-M'15) received his M.S. and Ph.D. in Telecommunications Engineering from the Universidad Politécnica de Valencia (UPV), Valencia, Spain, in 2012 and 2016, respectively.

From 2010 to 2016 he was with Grupo de Aplicaciones de Microondas, UPV, and collaborated with Aurora Software and Testing S.L. in the development of electromagnetic analysis CAE tools, along with high-power filters and multiplexers. In 2013 he was a visiting researcher at the University of Maryland, College Park, MD. In 2016 he was with the

Technische Universitaet Graz, Graz, Austria, developing microwave ceramic filters with additive manufacturing. In 2017 he joined the Semiconductor Components Group at Kyocera International, San Diego, CA, where he currently develops next-generation T/R modules and electronics packaging for active phased array radars.

Dr. Carceller was a recipient of the Fall 2009 IEEE Microwave Theory and Techniques Society (IEEE MTT-S) Undergraduate Scholarship.



**Jesús Ruiz Garnica** was born in Tarragona, Spain, in 1986. He received the B.S. degree in Telecommunication Engineering in 2012, and the M.S. degree in Communication Systems, Technologies and Networks in 2014, all of them from the Universidad Politécnica de Valencia. He is currently working towards the Ph.D. degree at the same university.

In 2014, he held a trainee position with Val Space Consortium (VSC), in Valencia, Spain, where he was involved in the design of microwave passive devices for high power applications in satellite communications. In 2015, he became a Researcher at the Instituto de Telecomunicaciones y Aplicaciones Multimedia (iTEAM), Universidad Politécnica de Valencia. His current research interests include the design of novel passive waveguide components.

**Jaione Galdeano**, photograph and biography not available at the time of publication.



**David Raboso** born in Alcazar de San Juan (Ciudad Real) in 1967, studied physics at the Autonomous University of Madrid. In 1992 he joined Payloads Systems Division of the European Space Agency (ESA) in the Netherlands where he became responsible for all activities related to RF breakdown in space microwave components. In 2002, he completed a Master degree in Space Engineering given by the University of Delft in the Netherlands. His participation in space programs is extensive starting with pioneer observation satellites to modern interplane-

tary missions such as Mercury (Bepi-Colombo) or navigation constellations (Galileo).

Mr. Raboso has co-authored over one hundred articles in prestigious journals and scientific conferences and is co-inventor on nine patents. Since 2010 he is chairman of the international conference covering issues of RF breakdown and passive intermodulation (Mulcopim) as well as ESA's responsible for updating the standards related to this discipline. In June 2010, after 18 years in Holland, he was assigned to direct the joint ESA-VSC European laboratories in high power RF and space materials in Valencia.